

Steady State Heat Transport by Microbubble Dispersions Mediating Convection With Phase Change Dynamics

William B Zimmerman

Correspondence: William B Zimmerman, Mappin Street, Sheffield S1 3JD, UK.

Received: November 7, 2021 Accepted: March 25, 2022 Online Published: April 14, 2022

doi:10.5539/ijc.v14n1p30

URL: <https://doi.org/10.5539/ijc.v14n1p30>

Abstract

A new theory for additional heat transfer convected by a dispersed phase of microbubbles was posited recently. An additional convection term in the heat transport equation reflects the latent heat of vapor of the liquid carried by the microbubbles from hot zones that vaporize more liquid to cold zones where condensation releases the latent heat. This theory was shown to be consistent with analysis of observations of freezing times measured by in the original Mpemba effect study, by inferring heat transfer coefficients fitted by Newton's law of cooling. In this paper, the scaling analysis, leading to the proposition that the additional heat flux is proportional to the phase fraction of microbubbles, is tested by steady state solutions of the canonical hot wall / cold wall buoyant convection problem. For phase fractions 0.02 and 0.1, the maximum ratio of additional Nusselt number emergent is five, occurring in the microfluidic regime. Increasing the characteristic length of the domain maintains the monotonicity of the increase in additional Nusselt number ratio over the case of no microbubbles present. The additional heat transfer due to the microbubble dispersion, ranging from 5-50%, is found to be nearly proportional to the microbubble phase fraction for the range of 0.02 to 0.2. However, larger characteristic lengths introduce insufficient heat flux from the hot wall to maintain a "driven cavity" flow structure, so that the steady state structure that emerges is a stable stratification with thin boundary layers near the hot and cold walls, with weak shear flow convection. The stable stratification resultant at higher characteristic lengths suppresses the additional heat flux due to microbubble mediation, but only moderately deviating from proportionality.

Keywords: phase change energy storage, microbubbles, direct contact heat transfer, evaporators, condensers.

1. Introduction

Microbubbles are famous for increasing mass transfer, especially useful in fermentation processes (see Gilmour and Zimmerman (2020)), yet do not have the same efficacy at heat transfer due to a complication. Generally, the solvents that are utilized where heat transfer is desirable are volatile. This additional heat transferred by hot microbubbles is partitioned between sensible heat transfer to the liquid or to provide the latent heat for evaporation of the solvent. Zimmerman et al. (2013) exploited this possibility by observing that microbubbles achieve internal homogeneity and equilibration with their gas-liquid interface within a few milliseconds of contact time from injection. By arranging that the liquid layer height limits the contact time to within that regime of maximum vaporization, without any time for sensible heat transfer, thermal *non-equilibrium* can be maintained with much higher vaporization rates than conventional boiling.

Isothermal distillation is possible, which is important for thermally unstable chemical composition of the solvent or suspended materials, such as microbes, that are thermally sensitive. Many other uses in chemical and biological processing are reviewed in Gilmour and Zimmerman (2020). The target in this paper is direct contact heaters / condensers such as those reviewed by Ribeiro and Lage (2004,2005), but with the novel introduction of microbubbles replacing conventional fine bubbles.

However, Zimmerman (2021) posited that most contacting configurations for microbubbles would achieve vapor-liquid equilibria as the contact time would naturally exceed those few milliseconds. The direct contact condenser has potential for exploitation of heat transfer by microbubbles. That paper posited an additional benefit to the obvious high gas-liquid interfacial area (therefore potential high interfacial heat transfer) and the high bubble flux (potentially hectares per cubic meter per second). Microbubbles that pass through a hot zone or near a heated surface will quickly vaporize, within milliseconds, to the saturation pressure, while absorbing the latent heat. Similarly, as they approach a cold surface or pass through a cold zone, they will condense the vapor, and release the associate latent heat. Zimmerman (2021) derived, from control volume analysis, an additional convection term for the heat transport equation.

Using scaling analysis, it was deduced that the additional convective term would introduce an additional heat flux that is proportional to the microbubble phase fraction, as well as an estimate of the constant of proportionality. The hypothesis

was supported by analyzing the time to freezing transient experiments of Mpemba and Osborne (1969) with boiled water. The heating rates were found to correlate linearly with the inverse solubility of oxygen at the initial temperature, reflecting that the microbubble phase had equilibrated with the dissolved gas composition in the liquid. The purpose of this paper is to test, for steady state solutions to the canonical hot wall/cold wall problem, called heat transfer in a slot with differential side wall heating, detailed in the classic book of Turner (1979), whether the scaling analysis of the modified heat transport equation holds, i.e. the additional heat flux is proportional to the microbubble phase fraction. Of course, the classical hot wall / cold wall problem is treated here with a microbubble dispersion in water, rather than a simple fluid.

Microbubbles have only been used in heat transfer dynamics since the seminal study of Zimmerman (2013), with the intention of minimizing heat transfer effects and maximizing solvent evaporation or binary distillation in sequels. In this paper, the intention is to characterize the level of additional heat transfer in water due to dispersions of air microbubbles, by exploiting phase change—evaporation in hot liquid near the hot wall, condensation in cold liquid near the cold wall.

The paper is organized as follows. In Section 2, the modifications to the hot wall / cold wall canonical problem are set out in the governing equations, following Zimmerman (2021), and subsequently simulated using Galerkin finite element methods with a spatially resolved mesh, for a wide range of domain sizes in the laminar flow regime. In Section 3, the results are represented and discussed. In Section 4, the conclusions are drawn.

2. Methodology: Buoyant Convection Modelling

Coupling momentum transport and heat transport is a well studied area of transport phenomena. The governing equations are

$$\begin{aligned} \rho \frac{\partial \mathbf{u}}{\partial t} + \mathbf{u} \cdot \nabla \mathbf{u} &= -\nabla p + \mu \nabla^2 \mathbf{u} + \rho \mathbf{g} \\ \frac{\partial \rho}{\partial t} + \nabla \cdot \rho \mathbf{u} &= 0 \quad \rho c_p \left(\frac{\partial T}{\partial t} + \mathbf{u} \cdot \nabla T \right) = \kappa \nabla^2 T \end{aligned} \quad (1)$$

Here, the dependent variables are described as follows: \mathbf{u} is the velocity vector, p is the pressure, and T is the temperature. The independent variables are spatial coordinates (implied in the differential operators) and time t . Everything else is a parameter ($\mu, \rho(T), c_p, \kappa, \mathbf{g}$) with fixed value once the fluid and venue are selected. If there is no imposed moving boundary or pressure gradient, then the motion is created by temperature gradients. Zimmerman (2021) proposed, from control volume analysis of cycling the evaporation and condensation dynamics, a modified heat transport equation for a dispersed microbubble phase in volatile liquid:

$$\rho c_p \frac{DT}{Dt} = \kappa \nabla^2 T - \phi \nabla \cdot \mathbf{u} F = \kappa \nabla^2 T - \phi F \nabla \cdot \mathbf{u} - \phi \mathbf{u} \cdot (\nabla F) \quad (2)$$

There are two additional terms once the extra divergence term is expanded. ϕ is the volume or phase fraction of microbubbles. $F(T)$ is a state function which has the connotation of the additional energy potential that is convected by the flow representing the latent heat of vaporization for the amount of vapor (of the volatile liquid) in the dispersed microbubble phase, per unit volume:

$$F(T) = c^*(T) \Delta H_v(T) = \frac{p^*(T)}{RT} \Delta H_v(T) \quad (3)$$

$p^*(T)$ is the saturation pressure of the liquid at the absolute temperature T . For simple volatile liquids, the saturation pressure is tabulated and well correlated by the Antoine equation. R is the gas constant. { XE "buoyant convection" }

$\Delta H_v(T)$ is the latent heat of vaporization, also commonly tabulated for volatile liquids, and commonly correlated by polynomial fit.

Equations (1) and (2) are commonly simplified by the Boussinesq approximation for buoyant convection, and non-dimensionalized by adopting scalings for length (h , the characteristic length scale), time ($\frac{\rho_0 c_{p,0} h^2}{\kappa}$), and velocity ($\frac{\mu_0}{\rho_0 h}$).

With these scalings, the system of equations (1) modified by (2) becomes:

$$\begin{aligned} \frac{\partial \mathbf{u}}{\partial t} + \mathbf{u} \cdot \nabla \mathbf{u} &= -\nabla p + \text{Pr}(T) \nabla^2 \mathbf{u} - \text{Gr} \hat{\rho}(T) \hat{\mathbf{k}} \\ \nabla \cdot \mathbf{u} &= 0 \\ \frac{DT}{Dt} &= \nabla^2 T - \phi N_{\text{Mpemba}}(T) \mathbf{u} \cdot \nabla T \end{aligned} \tag{4}$$

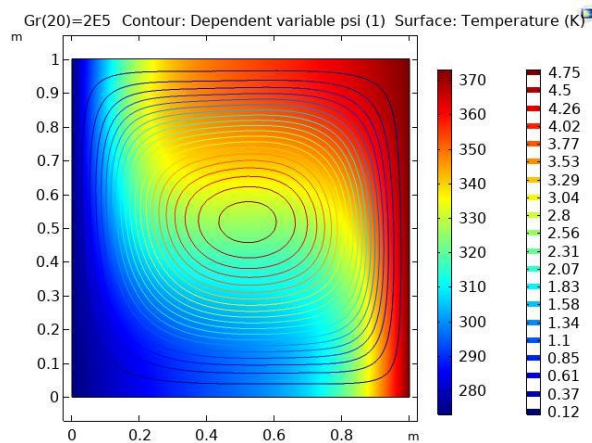


Figure 1. Streamfunction and temperature profile for the steady state solution to (4) for water with $Gr=2 \times 10^5$ ($h=1.43\text{mm}$) in the hot wall-cold wall problem on a unit square. No microbubble phase, i.e. $f=0$

The PDE engine used is Comsol Multiphysics v. 5.6. An exemplar solution for $Gr=2 \times 10^5$ with grid convergence found by using an extremely fine mesh with 26254 elements (236064 degrees of freedom) is shown in Figure 1. A mesh resolution study showed convergence to the at least three significant figures in the Nusselt number – the emergent global feature characterizing heat flux across either the hot or cold walls.

As illustrated in Zimmerman (2006), such steady state buoyant convection problems must be solved by parametric continuation in the nonlinearity parameter Gr . For a fixed liquid, such as water, Gr has the interpretation of being controllable by changing the size of the square. For instance, with water, $Gr=10^{13}$ corresponds to a side of $h = 52.7\text{cm}$ for the square domain. Typically, the parametric continuation for (4)-(5) takes 200~300 logarithmic steps to achieve $Gr \sim 10^{13}$. Because of the cubic dependence on h in Gr , for most of the parametric continuation, the hot wall-cold wall domain is very small, achieving microfluidic scales around $Gr \sim 10^{4-6}$. Figure 1 is representative of this range.

The Prandtl number for water can be found from the NIST database of liquid properties and represented as a cubic spline interpolation function. The steady state of the model equations (4) and (5) are solved by the Galerkin finite element

method for the hot wall-cold wall problem, where the hot wall is held at fixed temperature $T_1 = 373\text{K}$ and cold wall

$T_1 = 273\text{K}$, on the unit square with upper and lower boundaries as no flux surfaces. This is described in section 3.2 of

Zimmerman (2006) for the simpler convection situation with constant Prandtl number for water and vanishing N_{Mpemba} .

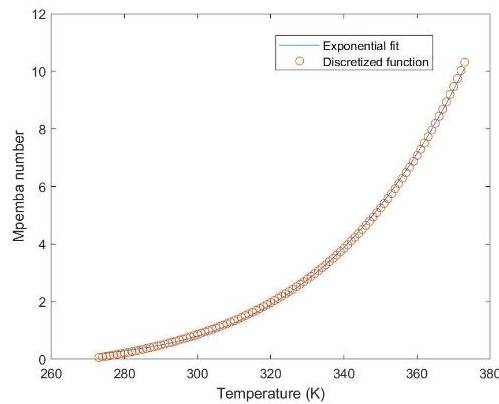


Figure 2. $N_{Mpemba} = \frac{F'(T)}{\rho_0 c_{p,0}}$ plotted against absolute temperature for water, along with the exponential fit, where the

“0” reference state are the properties of water at 20°C. Right: Streamfunction and temperature profile for the steady state solution to (4) for water with $Gr=2 \times 10^5$ ($h=1.43\text{mm}$) in the hot wall-cold wall problem on a unit square. No microbubble phase, i.e. $\phi = 0$

\hat{k} is the unit vector in the positive (antiparallel gravity) direction. $\hat{\rho}(T)$ is the specific gravity of water, taken from Zimmerman (2006) as an interpolation function via cubic splines. There are three dimensionless functions / parameters governing the dynamic similarity { XE "dynamical similarity" } of the problem: (i) the Mpemba number is defined in the caption of Figure 1, expressing the novel component of this buoyant convection analysis due to transport of the latent heat via the microbubble phase; (ii) the Prandtl number { XE "Prandtl number" } that is a function of the fluid and temperature; (iii) the buoyancy group { XE "Rayleigh number" } that gives the relative importance of gravitation to dissipative mechanisms:

$$Pr(T) = \frac{\mu(T)c_p(T)}{\kappa(T)}; \quad Gr = \frac{\rho_0^2 c_{p,0} g h^3}{\mu_0 \kappa_0} = \frac{g h^3}{\nu_0 \alpha_0} \tag{5}$$

3. Results and Discussion

Figure 1 and Figure 3 present a set of steady state solutions for streamlines and temperature profiles for parametric series of gravity group $Gr = (2 \times 10^6, 2 \times 10^6, 2 \times 10^9, 2 \times 10^{11}, 2 \times 10^{13})$ which span the equivalent side length of millimeter to half meter scale. This parametric series is a subset of the 200-300 solutions swept so that convergence is found for each subsequent value via parametric continuation. Of course, the reason parametric continuation is necessary is that gravity group Gr is a proxy for the level of nonlinearity in the dynamics. Highly nonlinear solutions are difficult to find without starting nearby in the basin of attraction for the solution via the multidimensional Newton’s method employed for iterative convergence by the PDE engine.

Figure 1 has the “bullseye” shaped streamlines consistent with the canonical lid driven cavity problem (see Zimmerman, 1998) and a temperature profile moderately different from the linear temperature gradient of pure conduction. The hot (red) regime has started to extend over the top, while the cold (blue) regime is spreading over the bottom of the domain. On average, the vertical profile is now density stably stratified, i.e. hot less dense water over cold more dense water. Figure 3(top) continues this development with further spreading of the hot zone at the top and the cold zone at the bottom, as the streamlines become asymmetric. Figure 3(second frame) shows that as Gr increases, the development of the stable stratification becomes dominant. The hot wall has a very thin boundary layer that is hot liquid, practically partitioned from the main stratified shear flow by an interposed cold layer. That interposed cold layer (and the squashed hot, near wall liquid layer) become thinner and thinner at the higher Gr group values in the bottom panels of Figure 3. By $Gr \sim 10^{13}$, the stratification seems nearly total, with barely visible boundary layers near the hot and cold walls. Simulation

above $Gr \sim 10^{13}$, requires refining the mesh further, especially near the hot and cold walls to resolve the thinning boundary layers, and re-starting parametric continuation from very low Gr values – computationally expensive. Although these four simulations were conducted with $\phi = 0.02$, it should be noted that all four microbubble phase fractions, including $\phi = 0$, result in visually indistinguishable flow and temperature profiles.

To distinguish among the heat transfer dynamics for variation of microbubble phase fraction, some other metric than the steady state temperature profile is necessary. The common metric is the Nusselt number, which has the interpretation of the total heat transfer across a boundary relative to the conductive heat transfer. At steady state, since there is no accumulation of heat in the domain, the total heat transfer across all boundaries nets to zero. As the upper and lower boundaries are no flux boundaries, the choice to compute the Nusselt number is arbitrary between the hot and the cold wall. For convenience we take the cold wall. The Nusselt number is then defined, as applied to this geometry, is

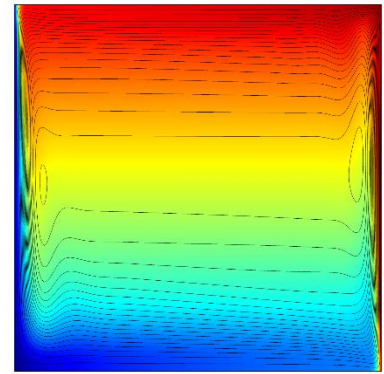
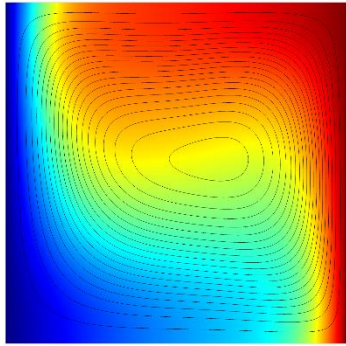
$$Nu = \frac{\int_{\partial B} q_{tot} dS}{\int_{\partial B} q_{cond} dS} = \frac{\int_0^1 \hat{n} \cdot \nabla T dy}{\int_0^1 \Delta T dy} = \frac{1}{T_1 - T_0} \int_0^1 \frac{\partial T}{\partial x} dy \quad (6)$$

Figure 4 is the log-log plot of Nusselt number Nu against the gravity group Gr for four different values microbubble phase fraction $\phi = 0, 0.02, 0.1, \text{ and } 0.2$. It is clear that the heat transfer rate monotonically increases with microbubble phase fraction, as the curves are parallel, but too close to discern the variation with ϕ . This is better achieved by a relative comparison, which uses the ratio of the Nusselt number in the presence of microbubbles to the Nusselt number in absence of microbubbles, Figure 5.

Figure 5 clarifies that the predicted scaling of the additional microbubble mediated heat flux is nearly proportional to the microbubble phase fraction for the maximum increase, which occurs in the microfluidic regime with $Gr \sim 10^6$. Thereafter, it is clear from the temperature / streamfunction profiles in Figure 3 that the fluid becomes density stratified, with the strength of stratification increasing as $Gr \sim 10^{11}$. It is not clear from the profiles whether or not the stratification strength continues to rise above this level, as the profiles are only modestly different. The monotonic response to ϕ is apparent as the curves are non-intersecting and parallel in behavior. The maximum increases are $\sim 5\%$, 25% , and 45% which are close to linearly related to ϕ .

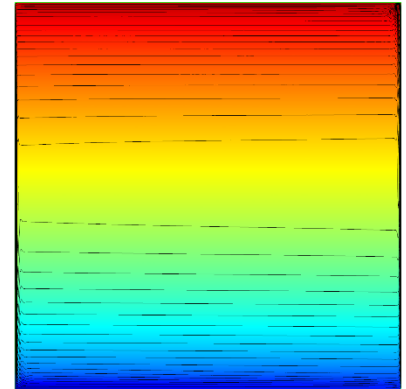
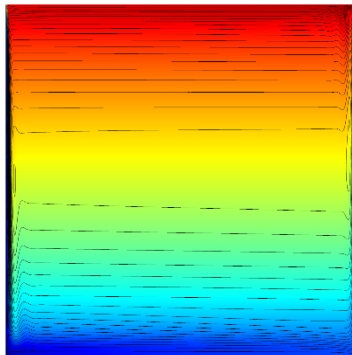
Of course, there is a rationale for why the stratification forms and then grows stronger. It is well known that in microfluidic transport, the surface area to volume of the fluid duct is very large. Zimmerman (1999) analyzed the formation of stable stratification in solutions where the density is a strong function of solute concentration, including ideal solutions as well as non-ideal, even non-monotonic mixing rules. In scenarios where stirring is introduced, if the stirring is sufficiently weak, then stable stratifications form that minimize the integrated density within the domain.

(a)



(b)

(c)



(d)

Figure 3. Steady state solutions with a parametric series in gravity group (a) – (d) ($Gr = 2 \times 10^6, 2 \times 10^9, 2 \times 10^{11}, 2 \times 10^{13}$) which can be thought of as simply changing the length of the side to ($h = 3.1\text{mm}, 3.1\text{cm}, 14.3\text{cm}, 52.7\text{cm}$) with $\phi = 0.02$. All four values of $\phi = 0, 0.02, 0.1, \text{ and } 0.2$ that were trialed have visually identical temperature and streamfunction profiles. Red represents $T=373\text{K}$ and dark blue $T=273\text{K}$. The streamlines are twenty uniformly spaced level sets of streamfunction from zero (the walls) to the maximum value (different in each case).

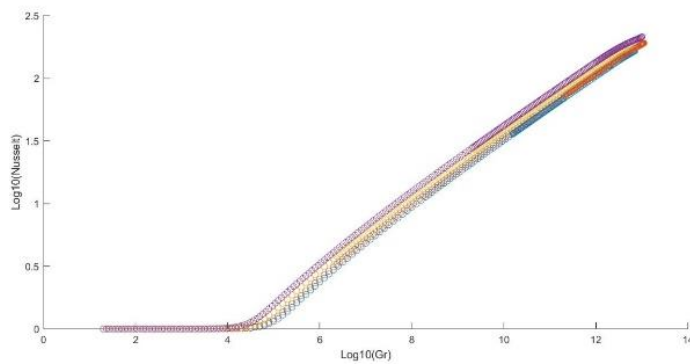


Figure 4. Common logarithm of the Nusselt number plotted against the common logarithm of the gravity group Gr for four different values microbubble phase fraction $\phi = 0, 0.02, 0.1, \text{ and } 0.2$. The lowest curve is $\phi = 0$, with Nusselt number monotonically increasing with ϕ . Because the log-log plot diminishes the distinguishability of small percentage differences in values, only this monotonic increase is a discernible trend. It should be noted that grid dependency becomes an issue for $Gr > 10^{12}$, as the boundary layers near the hot and cold wall become very thin.

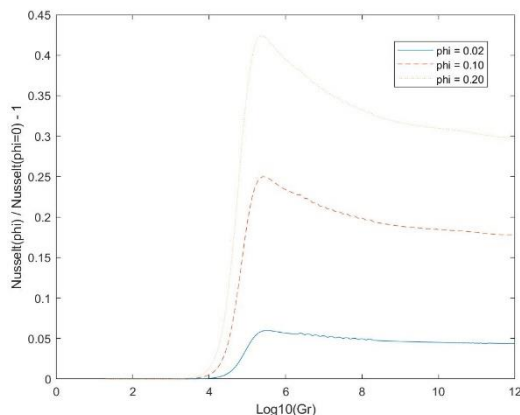


Figure 5. Fractional change in the ratio of Nusselt numbers for ϕ relative to $\phi=0$, plotted against the common logarithm of the gravity group Gr for three different values microbubble phase fraction $\phi = 0.02, 0.1, \text{ and } 0.2$. The lowest curve is $\phi = 0.02$, with Nusselt number monotonically increasing with ϕ . From the microfluidic scale of $Gr \sim 10^4$, the additional convective flux due to the microbubble phase rises rapidly, peaking in the millimeter scale $Gr \sim 10^6$, before plateauing with a minor decay over the next six decades, before grid dependency becomes an issue.

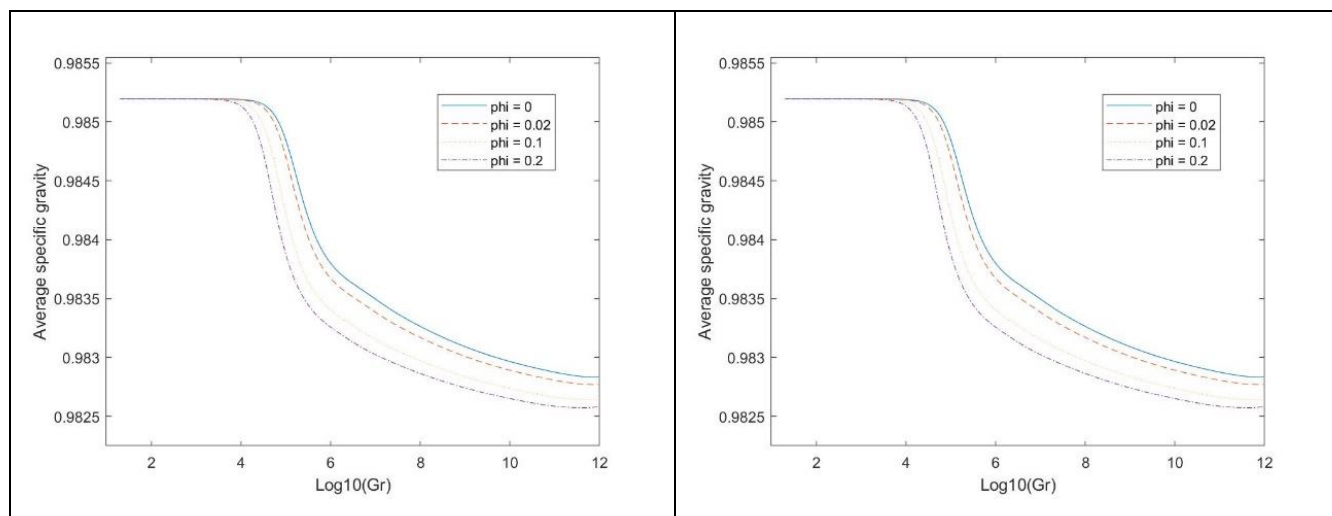


Figure 6. (top) Volume-averaged specific density with Gr variation for selected ϕ values. (bottom) Volume-averaged temperature with Gr variation for selected ϕ values

As the stirring rate increases, the kinetic energy can lift the solute so that a steady solution achieves greater than the minimum integrated density. In this heat transfer analogue, the stirring kinetic energy is injected proportional to the surface area of the hold wall, hence why the Nusselt number rises with increasing Gr. However, the total mass rises proportional to the volume of the duct. So eventually, the stirring force is insufficient to lift the mass to higher potential energy as Gr rises, so the temperature field (solute) is arranged to minimize the energy integral, i.e. the stable stratification suppresses convective mixing / heat transport.

Figure 6 makes clear that increasing ϕ increases the strength of the stable stratification as it achieves lower average specific gravity – starts the formation of the stable stratification at lower Gr values and accelerates the stabilization with increasing ϕ and Gr. This is a direct consequence of better heat transfer, as the bottom frame of Figure 6 illustrates. Average temperature also rises with increasing ϕ and Gr. The microfluidic range, $Gr \sim 10^4-6$, shows exponential increase in strength of the stable stratification / average temperature, before both

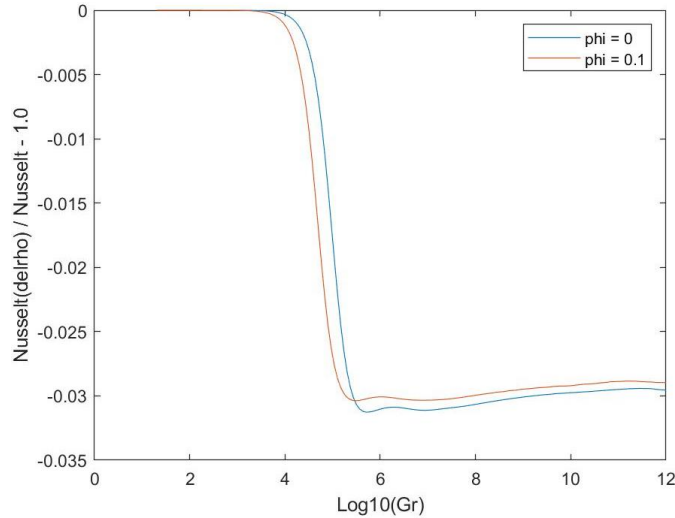


Figure 7. Modifying the specific gravity for the air saturation of water influence according to the correlation of Watanabe and Iizuka (1985). Fractional change in the ratio of Nusselt numbers for fixed ϕ , plotted against the common logarithm of the gravity group Gr for three different values microbubble phase fraction $\phi = 0.0$, and 0.1 . The lower curve is $\phi = 0$.

level off in the millimeter scale, with a constant plateau achieved in the meter scale. Zimmerman and Rees (2007) studied the double diffusion problem with initial stable stratification, but strong sidewall heating. In the transient situation, the stable stratification can be overturned by sufficiently strong heating, as the stratification strength depends on solute distribution.

One area of speculation is the role of the change in specific gravity of water due to air saturation. Watanabe and Iizuka (1985) carefully measured the change in specific gravity of water with saturated, dissolved air, as a function of water temperature. Their cubic polynomial correlation was used to modify $\hat{\rho}(T)$ for temperatures below 53°C , the neutral change temperature (they measured between 0 and 45°C). Oxygen and nitrogen solubility fall off dramatically above 53°C , so there is negligible contribution above this level. This translates into a piecewise cubic polynomial modifying equations (4).

$$\Delta\hat{\rho}(T) = \begin{cases} -5.252 \times 10^{-3} + 1.474 \times 10^{-4}T \\ -3.0689 \times 10^{-6}T^2 \\ + 4.0688 \times 10^{-8}T^3, & T < 326\text{K} \\ 0, & T > 326\text{K} \end{cases} \quad (7)$$

As the average temperature in the domain typically varies between 323K and 332K (cf. Figure 6) with increasing Gr in the range explored, the average effect of air saturation on changing density is typically around -6×10^{-4} . However, it is the spatially distributed effect that is of concern in the free convection dynamics explored here. Figure 7 illustrates that the maximum change in Nusselt number due to the density change from air-saturation is approximately a 3% decrease, which plateaus above $\text{Gr} \sim 10^6$. However, as found for all ϕ values, the change with Nusselt number is indistinguishable visually. Compare Figure 8 with Figure 5 to see that there is no discernible *relative* difference to the effect of microbubble phase fraction ϕ . Zimmerman (2021) argues that the thermal diffusivity increases with uniformly dispersed ϕ according to common mixing rules, but as in all length scales of interest, convection dominates the contribution to the Nusselt number, negligible effect will arise from considering the thermal diffusivity dependence on microbubble phase fraction.

This is perhaps the largest buoyancy effect that is unaccounted for in this model – the effect of the two phase density on the phase fraction of microbubbles. However, the assumption underpinning the treatment in this paper is that microbubble phase fraction is uniformly distributed spatially. Undoubtedly, for any real steady state convection with dispersed microbubbles, the volume increases in warm zones and decreases in cold zones due to the vaporization and condensation, respectively. Treating these two contributions to density variation would require adding the heat transport (and consequential changes to mass transport) effects of (4) to the bubbly flow and mass transport model of Al-Mashhadani et

al. (2015) – beyond the scope of this paper.

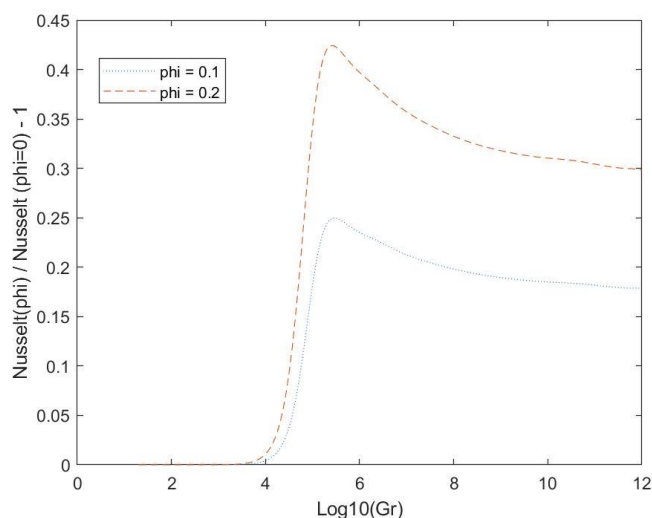


Figure 8. Modifying the specific gravity for the air saturation of water influence according to the correlation of Watanabe and Iizuka (1985). Fractional change in the ratio of Nusselt numbers for ϕ relative to $\phi = 0$, plotted against the common logarithm of the gravity group Gr for three different values microbubble phase fraction $\phi = 0.1$, and 0.2 .

The lower curve is $\phi = 0.1$.

4. Conclusions

The hypothesis of proportionality between the additional heat transfer and the microbubble phase fraction holds within the microfluidic range of flow cells, where convection dominates is proposed in Zimmerman (2021) as due to scaling analysis. The prediction is found to hold only closely in the microfluidic regime of steady state buoyant convection. Monotonic increase but less than proportionality holds with larger flow cell characteristic lengths where stable stratification forms under steady state conditions. The formation of the stable stratification dominates the heat transfer dynamics, which could be alleviated by continuous microbubble injection and removal, such as in the airlift loop open system, frequently adopted for bioreactors (Al-Mashhadani et al. (2015)).

Nonetheless, the predicted levels of additional heat transfer with the presence of a microbubble dispersion of air in water vary from 5-50% with the phase fraction of 0.02 to 0.2. These additional heat transfer rate are consistent with the decreases in the time to freezing observed by Mpemba and Osborne (1969). If they hold in other common heat transfer configurations such as bioreactors, heat pumps, and direct contact evaporators and condensers, substantial efficiency increases can be achieved with slight increase in processing costs due to injection of long lived microbubble dispersions.

NOMENCLATURE

c_p	[J/kgK]	Heat capacity at constant pressure
c^*	[mol/m ³]	Saturation concentration
F	[J/m ³]	Latent heat density within dispersed microbubbles
g, \mathbf{g}	[m/s ²]	Gravitational acceleration constant/vector
h	[m]	Side length for 2-D square domain
Gr	[-]	Non-dimensional gravity group parameter
$N_{Mpeмба}$	[-]	Dimensionless function of temperature
Nu	[-]	Non-dimensional ratio of total to conductive heat flux
p	[N/m ²]	Pressure scalar – dimensional or dimensionless (context)
P^*	[N/m ²]	Saturation pressure
Pr	[-]	Prandtl number (temperature dependent)
q	[W/m ²]	Heat flux
R	[J/molK]	Gas constant
T	[K]	Temperature – dimensional or dimensionless (context)
t	[s]	Time coordinate
\mathbf{u}	[m/s]	Velocity – dimensional or dimensionless (context)
x	[m]	Coordinate – dimensional or dimensionless (context)
z	[m]	Coordinate – dimensional or dimensionless (context)

Special characters

α	[m ² /s]	Thermal diffusivity
ϕ	[-]	Microbubble phase fraction
κ	[W/mK]	Thermal conductivity
$\hat{\mathbf{k}}$	[-]	Unit vector anti-parallel to gravity
$\hat{\mathbf{n}}$	[-]	Outward pointing unit normal to the domain
ρ	[kg/m ³]	Density
$\hat{\rho}$	[-]	Specific gravity (temperature dependent)
μ	[Pa·s]	Dynamic viscosity

Subscripts

0	Ambient or reference state
---	----------------------------

Acknowledgments

The author acknowledges the Engineering and Physical Sciences Research Council (EPSRC) for supporting this work financially (Grant no. EP/K001329/1, EP/N011511/1 and EP/S031421/1). This work was presented as part of a keynote address at the 15th International Conference on Heat Transfer, Fluid Mechanics, and Thermodynamics (HEFAT-15). A version was published as part of the conference proceedings.

References

- Al-Mashhadani, M. K. H., Wilkinson, S. J., & Zimmerman, W. B. (2015). Airlift bioreactor for biological applications with microbubble mediated transport processes. *Chem. Eng. Science*, *137*, 243-253. <https://doi.org/10.1016/j.ces.2015.06.032>
- Gilmour, D. J., & Zimmerman, W. B. (2020). Microbubble Intensification of Bioprocessing. *Advances in Microbial Physiology*, *77*, 1-35. <https://doi.org/10.1016/bs.ampbs.2020.07.001>

- Mpemba, E. B., & Osborne, D. G. (1969). Cool? *Phys. Educ.*, *4*, 172-175. <https://doi.org/10.1088/0031-9120/4/3/312>
- Ribeiro, C. P., & Lage, L. P. C. (2004). Experimental study on bubble size distributions in a direct-contact evaporator. *Braz. J. Chem. Eng.*, *21*(1), 69-81. <https://doi.org/10.1590/S0104-66322004000100008>
- Ribeiro, C. P., & Lage, L. P. C. (2005). Gas-Liquid Direct-Contact Evaporation: A Review. *Chemical Engineering and Technology*, *28*(10), 1081-1107. <https://doi.org/10.1002/ceat.200500169>
- Turner, J. S. (1979). Buoyancy effects in fluids. Cambridge University Press, Cambridge.
- Watanabe, H., & Iizuka, K. (1985). The Influence of Dissolved Gases on the Density of Water. *Metrologia*, *21*, 19. <https://doi.org/10.1088/0026-1394/21/1/005>
- Zimmerman, W. B. J. (2006). Multiphysics Modelling with Finite Element Methods, World Scientific Series on Stability. *Vibration and Control of Systems*, *18*, Singapore. <https://doi.org/10.1142/6141>
- Zimmerman, W. B. (1998). The effect of chemical equilibrium on the formation of stable stratification. *Appl. Sci. Res.*, *59*, 298-298. <https://doi.org/10.1023/A:1001147808516>
- Zimmerman, W. B., & Rees J.M. (2007). Rollover instability due to double diffusion in a stably stratified cylindrical tank. *Physics of Fluids*, *19*, 123604. <https://doi.org/10.1063/1.2827488>
- Zimmerman, W. B., Al-Mashhadani, M. K. H., & Bandulasena, H. C. H. (2013). Evaporation dynamics of microbubbles. *Chemical Engineering Science*, *101*, 865-877. <https://doi.org/10.1016/j.ces.2013.05.026>
- Zimmerman, W. B. (2021). Towards a microbubble condenser: Dispersed microbubble mediation of additional heat transfer in aqueous solutions due to phase change dynamics in airlift vessels. *Chemical Engineering Science*, *238*, 116618. <https://doi.org/10.1016/j.ces.2021.116618>

Copyrights

Copyright for this article is retained by the author(s), with first publication rights granted to the journal.

This is an open-access article distributed under the terms and conditions of the Creative Commons Attribution license (<http://creativecommons.org/licenses/by/4.0/>).